*Regular Article*

# Experimental and Theoretical Investigation of Corrosion Inhibitive Potentials of (E)-4-hydroxy-3-[(2,4,6-tribromophenyl)diazenyl]benzaldehyde on Mild Steel in Acidic Media

S.J. Amoko[a,b], O.F. Akinyele[b], O.E. Oyeneyin[d,*], D.S. Olayanju[b] and C.O. Aboluwoye[c]

*[a]Department of Chemistry, Adeyemi College of Education, Ondo State, Nigeria*

*[b]Department of Chemistry, Obafemi Awolowo University, Ile-Ife, Osun State, Nigeria*

*[c]Department of Chemical Sciences, Adekunle Ajasin University, Akungba-Akoko, Ondo State, Nigeria*

*[d]Theoretical and Computational Chemistry Unit, Department of Chemical Sciences, Adekunle Ajasin University, Akungba-Akoko,*

*Ondo State, Nigeria*

Corrosion of metal surfaces amongst other problems is one major disaster militating against proper functioning of the oil and gas and other manufacturing industries. To, therefore, lessen the risk, organic corrosion inhibitors have been applied to lessen the rate of corrosion and its effects. Therefore, the need to continually search for materials with corrosion inhibitive properties is imperative. (E)-4-hydroxy-3-[(2,4,6-tribromophenyl)diazenyl]benzaldehyde on mild steel in Aacidic media was synthesized and characterized *via* FTIR, UV-Vis and NMR ($^1$H and $^{13}$C) spectroscopy. Weight loss and potentiodynamic polarization methods were studied to determine the rate of corrosion (Cr) and percentage of inhibition efficiency (%IE). The mechanism of adsorption agrees with the Freundlich adsorption isotherm. The surface morphology of the mild steel was determined using the scanning electron microscopy (SEM) in the bi-condition of the presence and absence of inhibitor. Inhibition efficiency (IE) was varied with concentration and temperature. The results revealed that IE increased with high concentration of the inhibitor but reduced while the temperature was increased. The SEM revealed the formation of protective layer of the inhibitor attachment to the metal surface. The results from the experiments agreed well with those obtained from DFT methods. AD3 could therefore be used as an anticorrosive agent in the petroleum industry.

**Keywords:** Adsorption isotherm, Surface morphology, Density functional theory, Scanning electron microscopy

## INTTRODUCTION

Corrosion of metals occurs because of the metals' immediate environment and as a result of acids used during pickling, descaling and oil well acidification processes [1]. This has led to reduction in equipment lifetime, increased cost of production, loss of lives and properties [2]. An instance was published by NACE in 2002 that 276 billion US Dollars was reported lost in 1998 in the US. [3]. Also, in

1992, about 200 people died as a result of sewer corrosion explosion in Mexico [2]. All these agitated the need to prevent and reduce corrosion.

The use of corrosion inhibitors became popular because its advantages outweigh other previous methods. Organic inhibitors, especially those containing heteroatoms like O, N, S are preferred to their inorganic/organometallic analogues in that most of them are extensively conjugated [4,5], this gives room for improved reactivity. Weight loss [5,6], potentiodynamic polarization (PP) technique [5,6], electrochemical impedance spectroscopy [6,7], *etc*. are

_____
*Corresponding author. E-mail: emmanueltoba90@gmail.com

methods used to investigate corrosion rates ($C_r$) and inhibition efficiencies (%IE) of molecules. Details as to which mode of adsorption was observed are predicted by the isotherm models [5].

In our previous work, the $C_r$ and %IE of an organic dye, NAD, were investigated and reported to lessen $C_r$ [5]. Recently, quantum mechanical packages have been employed solely and in conjunction with experiments to investigate molecular properties, corrosion inhibition inclusive [4,5,8]. The DFT methods have been used to successfully and accurately predict the properties of organic systems [4,5,8]. Calculations were performed on the molecules using DFT (B3LYP) with 6-31G* basis set. This correlation was chosen to validate its consistency with experimental findings. Pure BLYP has been used to investigate molecular properties [9,10]. Also, the B3LYP has been used to a very large extent in past and in recent times for predicting molecular properties. An instance was reported for phenothiazine based organic π-conjugated molecules, where the molecular properties were accurately predicted using both BLYP and B3LYP correlations [9]. Also, the nonlinear optical properties of a D-A type 1-[4-({(E)-[4(methylsulfanyl)phenyl]methylidene}amino) phenyl] ethanone was predicted using DFT with BLYP and B3LYP correlations, their results were consistent with available experimental results [10].

Accordingly, in this study, a novel (E)-4-hydroxy-3-[(2,4,6-tribromophenyl)diazenyl]benzaldehyde on mild steel in acidic media (AD3) was synthesized and characterized *via* Fourier transform infrared (FTIR), ultraviolet/visible (UV-Vis) and nuclear magnetic resonance (^{1}H and ^{13}C NMR) spectroscopic techniques. Weight loss and potentiodynamic polarization (PP) techniques were employed to investigate the $C_r$ and %IE while the surface architecture of the MS specimens were scanned using a SEM/EDX analyzer after immersing in 1 M $H_2SO_4$ without (blank) and with the inhibitors. The MS specimens scanned were (i) shined metal (ii) metal with acid but without inhibitor (blank) and (iii) metal with acid and inhibitor. These molecules were modelled and optimized to obtain properties such as the frontier molecular orbitals (FMOs) [4]. Also, properties like the chemical hardness (η), dipole moment (μ), chemical softness (δ), global electrophilicity (ω) and fraction of electron transferred (ΔN) were calculated.

## MATERIALS AND METHODS

### Synthesis of AD3

The method reported in (Scheme 1) [11] was used to synthesize AD3. A suspension of 2,4,6-tribromoaniline (13.19 g, 40 mmol) in HCl (36 ml) and water (16 ml) was heated (70 °C) until it dissolved completely. This was followed by diazotization of the solution in an ice below 5 °C with sodium nitrite (2.8 g, 40 mmol) dissolved in water (10 ml). The solution was added slowly for 45 min at 0 °C to a solution of *p*-hydroxybenzaldehyde (4.88 g, 40 mmol) while stirring in water (75 ml) containing NaOH (1.6 g) and $Na_2CO_3$ (14.8 g). The orange solid product was recrystallized from ethanol after filtration and washed with water. The HCL solution was produced using the earlier procedure [5].

### Weight Loss Experiment

For this measurement, the mild steel coupons were weighed. The experiment was conducted inside a thermostated water bath wherein the coupons were dipped in 0.5 M HCl (100 ml) test solutions with varying inhibitor concentrations (100-500 ppm) for 6 h at different temperatures (298-338 K). The samples were brushed, washed with distilled water, rinsed in acetone and dried before reweighing [5,6]. $C_r$ (Eq. (1)), degree of surface coverage, θ (Eq. (2)) and the %IE (Eq. (3)) were obtained from the weight loss data:
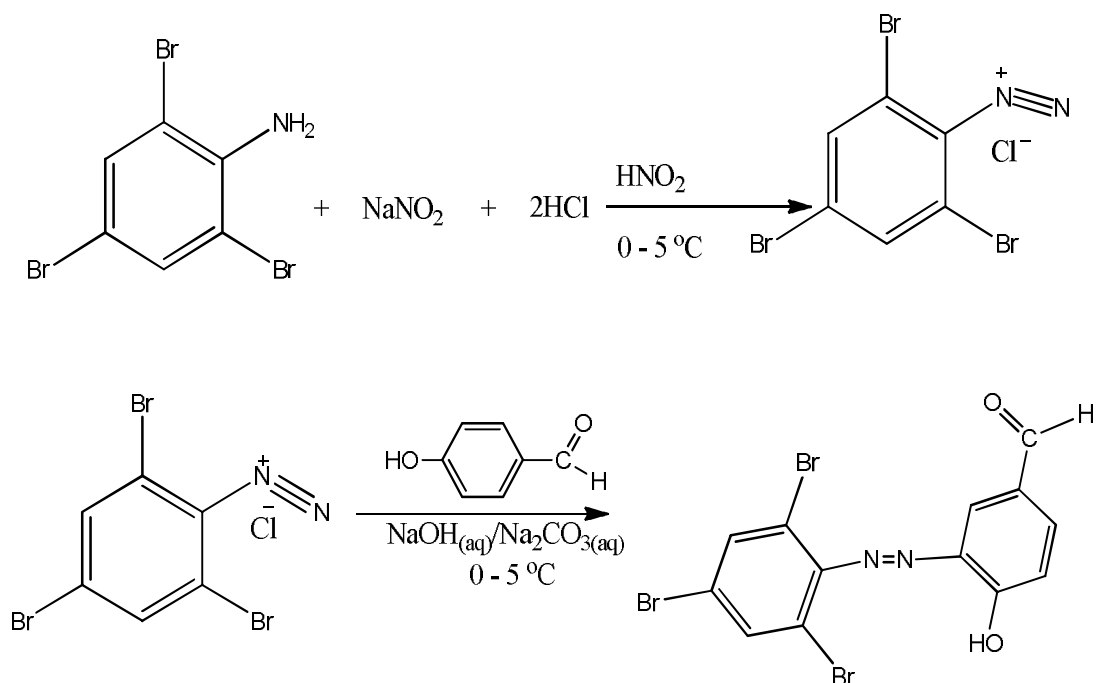
$$C_R = \frac{W_1 - W_2}{At} \tag{1}$$

$$\theta = 1 - \frac{C_r^i}{C_r^0} \tag{2}$$

$$\%IE = \theta \times 100 \tag{3}$$

where $W_o$ is the weight loss without the inhibitor, $W_1$ is the weight loss of mild steel with the inhibitor in grams, A is the area of the mild steel in $cm^2$, t is immersion time in h, $C_r i$ is the rate of corrosion with inhibitor, and $C_r o$ is the rate of corrosion without inhibitor in g $cm^{-2}$ $h^{-1}$.

Adsorption isotherms were employed in explaining the

*Scheme 1*. Preparation of AD3

substitution of the inhibitor on the metal surface. The Freundlich adsorption isotherm (Eq. (4)) was employed in this case [23,24]:

$$\log\theta = \log K_{Ads} + n\log C \tag{4}$$

where $C$ is the concentration of inhibitor, $K_{ads}$ is the equilibrium adsorption constant, and $\theta$ is the extent of surface coverage.

The thermodynamic parameters were investigated to further explain the adsorption process. The standard Gibbs free energies of adsorption ($\Delta G_{ads}^0$) were calculated [5,25] in Eq. (5),

$$K_{ads} = \frac{1}{55} e^{-\frac{\Delta G_{ads}^0}{RT}} \tag{5}$$

where R is the gas constant, $\Delta G_{ads}^0$ is the free energy of adsorption, and 55.5 value is the isocratic contribution of water in the solution. The enthalpy, $\Delta H°$ and entropy $\Delta S°$ were obtained from the plots of $\Delta G_{ads}^0$ against temperature (Eq. (6)) [5].

$$\Delta G_{ads}^0 = \Delta H^0 - T\Delta S° \tag{6}$$

Kinetic model was also employed in explaining the adsorption behavior of AD3 by calculating the activation energies, Ea, and the pre-exponential factors from the plot of lnCr against 1/T (Fig. 9), from the Arrhenius Eqs. (7) and (8), as presented in Table 3 [5,26].

$$C_R = Ae^{-\frac{E_a}{RT}} \tag{7}$$

$$\ln C_R = \ln A - \frac{E_a}{RT} \tag{8}$$

Enthalpy, $\Delta H^*$, and entropy, $\Delta S^*$, of activation values were calculated (Eq. (8)) [5], and the results are provided in Table 3,

$$C_R = \left(\frac{RT}{Nh}\right)\exp\left(\frac{\Delta S^*}{R}\right)\exp\left(\frac{-\Delta H^*}{RT}\right) \tag{9}$$

where h is the Plank constant, N is the Avogadro number, T is the absolute temperature and R is the universal gas constant.

## Electrochemical Measurements

The experiment of electrochemical measurements was conducted [5]. The inhibition efficiency was calculated from the data extracted from the Tafel curves (Eq. (10)) [12].

$$\%IE = \frac{I_{corr}^{0} - I_{corr}}{I_{corr}^{0}} \times 100 \tag{10}$$

where $I_{corr}^{0}$ and $I_{corr}$ are the corrosion densities in the absence and presence of the inhibitor, respectively.

## SEM Surface Analysis

The surface morphology of the mild steel after immersion and before immersion in 0.5 M HCl solution in the absence and presence of inhibitor was imaged using the Phenom Prox scanning electron microscope (SEM) by Phenomworld Eindhoven The Netherlands.

## Quantum Chemical Calculations

Quantum chemical calculations were carried out with complete geometry optimization using DFT with a large polar 6-31G* basis set for all atoms [4,5,13]. Electronic properties such as the $E_{HOMO}$ and $E_{LUMO}$, $\Delta E$, global reactivity descriptors like electronegativity $\chi$, $\eta$, S and $\Delta N$ were calculated from the results of the FMOs energies [4,5].

# RESULTS AND DISCUSSION

## IR Spectrum of AD3

The infrared spectrum (Fig. 1) of AD3 has a band at 3416 cm$^{-1}$ assigned to the OH vibration frequency [11,14]. Band at 3074 cm$^{-1}$ was assigned to sp$^{2}$ CH vibration of the aromatic ring [14] while the band at 1697 and 1614 cm$^{-1}$ were due to -C=O and -C=C- stretching vibrations, respectively. Also, the spectrum displays azo group (-N=N-) at 1456 cm$^{-1}$. The band at 1215 cm$^{-1}$ was assigned to C-O while band at 806 cm$^{-1}$ was due to the stretching band of C-Br group. The IR spectrum showed the expected

characteristics of bands signifying the formation of the dye.

## Electronic Spectra

Electronic absorption spectrum (Fig. 2) of AD3 showed three major peaks. Peak at 250 nm corresponds to π-π* aromatic transition, 325 nm due to n-π* and peak at 390 nm was assigned to the intermolecular charge transfer (IMCT) involving the whole molecule through the -N=N- group [15].

## Nuclear Magnetic Spectrum ($^{1}$H NMR and $^{13}$C NMR)

The $^{1}$H NMR spectrum of AD3 (Fig. 3a) was measured using d$_{6}$-DMSO solvent. The results showed a signal at 5.50 ppm which was assigned to the presence of proton of hydroxyl group. The same spectrum displays signal between 7.30-8.22 ppm attributed to the protons on the phenyl rings. The signal at 9.90 ppm was due to the aldehyde proton. The $^{13}$C NMR spectrum (Fig. 3b) showed signals at 107, 108, 150, 120, 128, 134, 135, 139, 144 and 150 ppm corresponding to the various aromatic carbons and at 162 ppm for the carbonyl carbon. Signals at 128 and 150 ppm were assigned to the carbons attached to the nitrogen atoms of the azo-group. The signal at 139 ppm was assigned to the carbon carrying the OH group, while the signals at 108 (for 2 equivalent carbons) and 115 ppm were assigned to carbons attached to bromine atoms.

## Weight Loss Measurements

Weight loss measurement for mild steel corrosion in the absence and presence of the studied azo dye were obtained at various concentrations and temperatures in 0.5 M HCl (Table 1).

The corrosion rate decreases with increase in the concentration of the inhibitor and increases at temperature. This may be due to the fact that as the concentration of the inhibitor increases, more of its molecules are adsorbed on the metal surface thereby causing more active site to be blocked by the inhibitor resulting in reduction of the corrosion rate.

Generally, in this work, the corrosion rate decreases with increase in the concentration of the inhibitors at each operating temperature. Hence, the increase in the inhibition efficiency as more inhibition molecules were adsorbed on
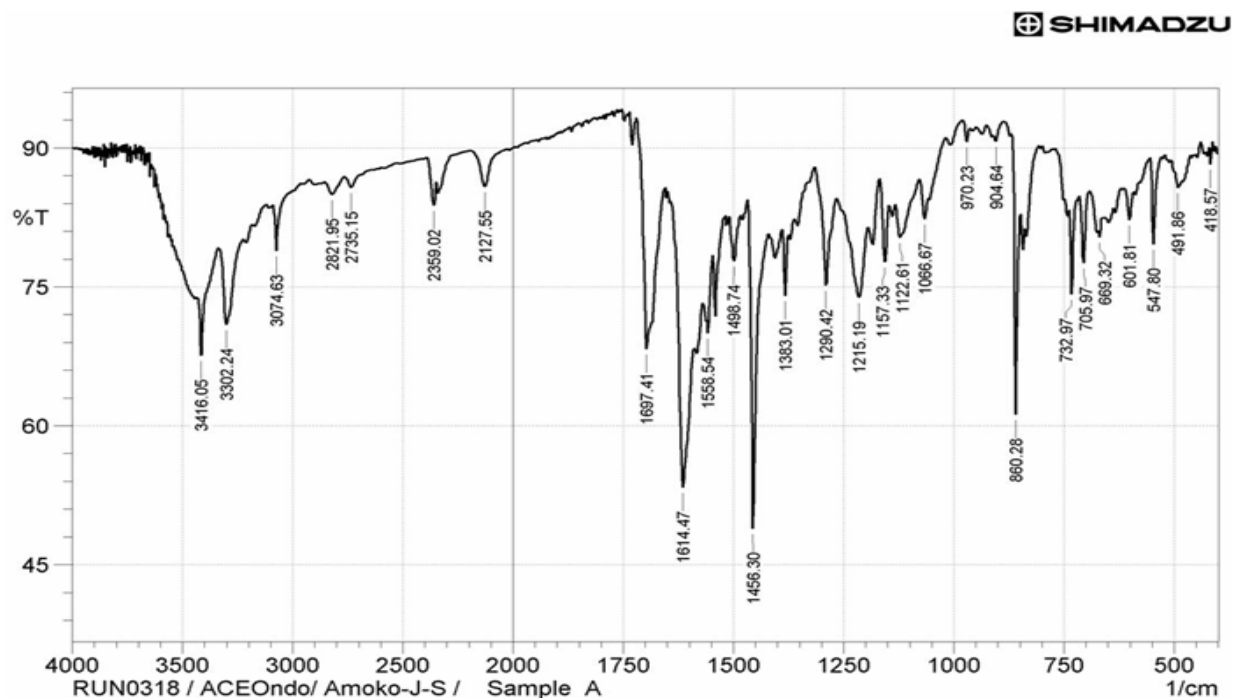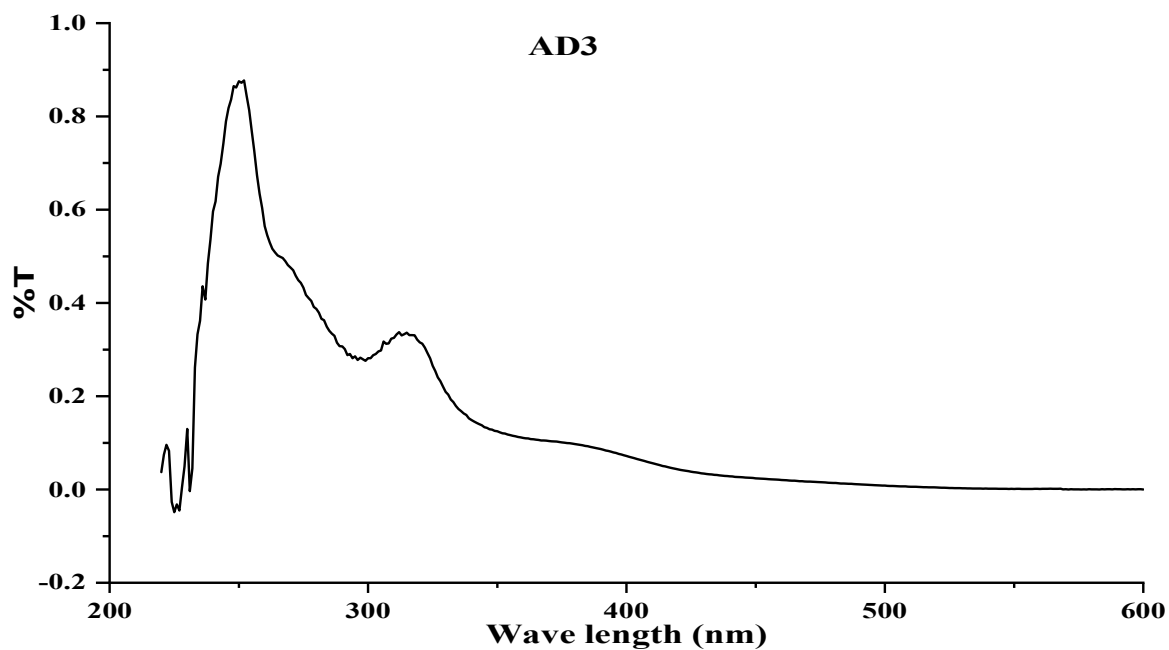
**Fig. 1.** IR spectrum of AD3.
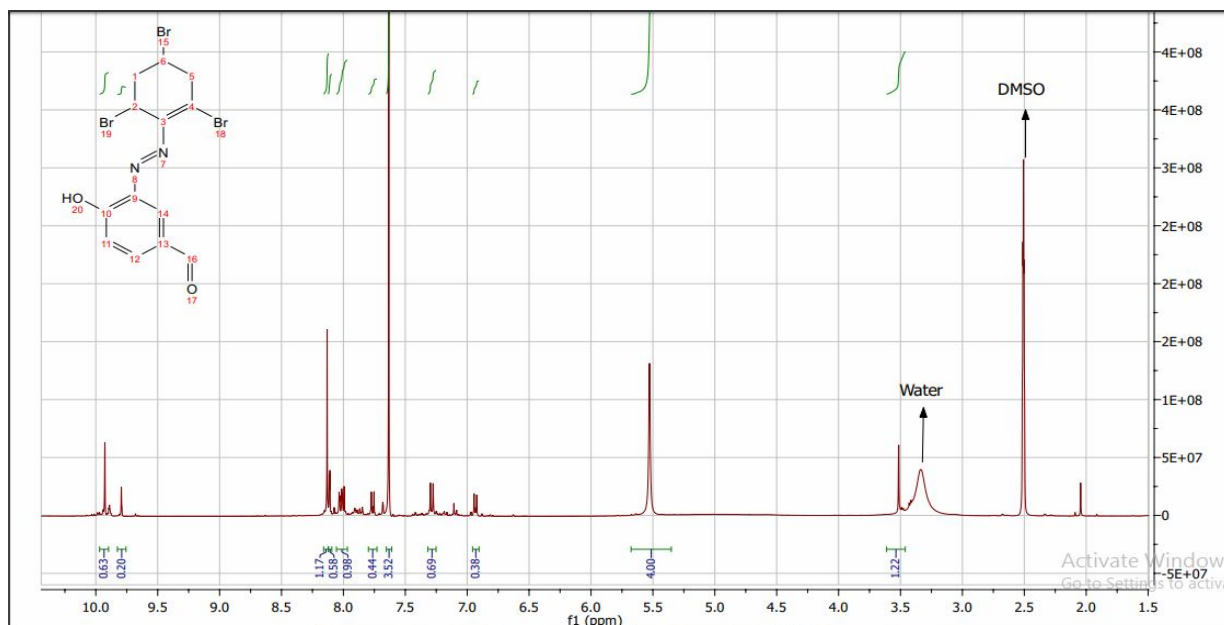


**Fig. 2.** UV-Vis spectrum of AD3.
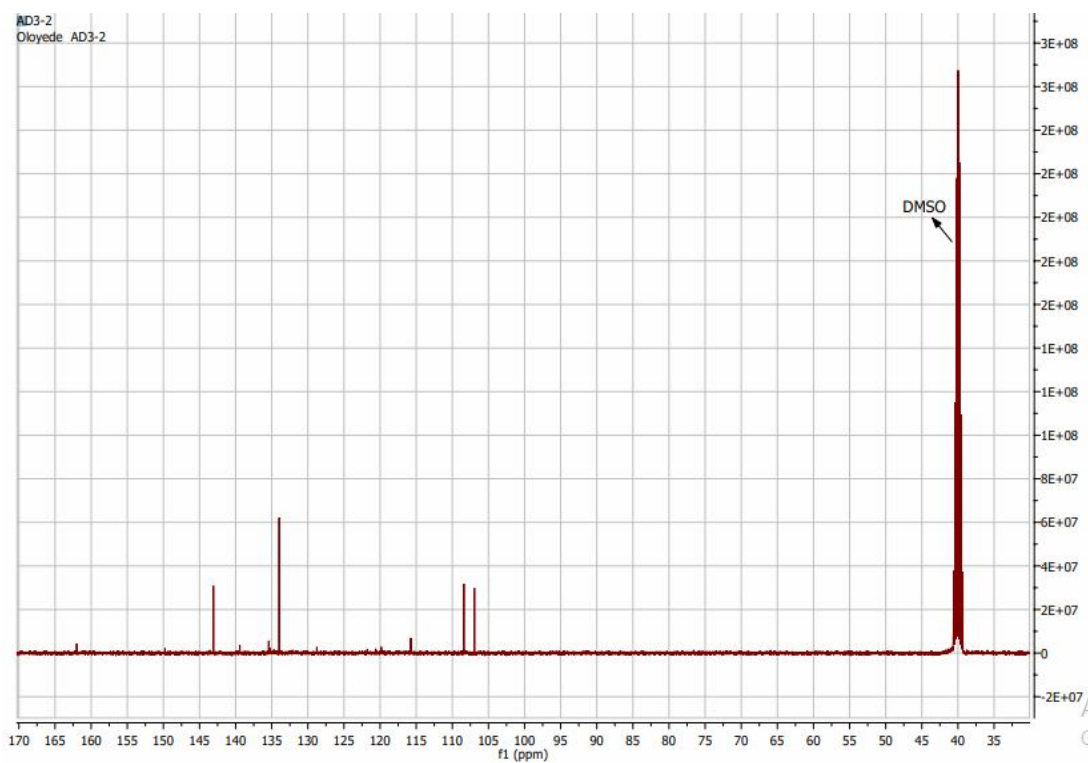
**Fig. 3a.** ^{1}H NMR of AD3.



**Fig. 3b.** ^{13}C NMR of AD3.

**Table 1.** Results Obtained from Weight Loss Analysis of AD3

| Temp. (K) | Concentration of the inhibitor (M) | Weight loss (g) | Corrosion rate ($g\ cm^{-2}\ h^{-1}$) | IE% | Θ |
|---|---|---|---|---|---|
| 298 | Blank | 0.041 | 0.002134134 | - | - |
| | 0.000216 | 0.0150 | 0.0009 | 58.14 | 0.581394096 |
| | 0.000432 | 0.0140 | 0.0008 | 61.95 | 0.619480713 |
| | 0.000648 | 0.0120 | 0.0007 | 65.40 | 0.654034532 |
| | 0.000864 | 0.0120 | 0.0007 | 67.23 | 0.672273855 |
| | 0.00108 | 0.0100 | 0.0006 | 73.27 | 0.732736357 |
| 308 | Blank | 0.036 | 0.002093207 | - | - |
| | 0.000216 | 0.0120 | 0.0007 | 68.30 | 0.682997228 |
| | 0.000432 | 0.0100 | 0.0006 | 72.68 | 0.726804394 |
| | 0.000648 | 0.0100 | 0.0006 | 73.50 | 0.734955291 |
| | 0.000864 | 0.0100 | 0.0005 | 75.31 | 0.753076559 |
| | 0.00108 | 0.0070 | 0.0004 | 80.39 | 0.803911106 |
| 318 | Blank | 0.048 | 0.002530798 | - | - |
| | 0.000216 | 0.0260 | 0.0014 | 46.60 | 0.466048226 |
| | 0.000432 | 0.0190 | 0.0011 | 55.11 | 0.551053988 |
| | 0.000648 | 0.0150 | 0.0009 | 65.06 | 0.650605794 |
| | 0.000864 | 0.0130 | 0.0007 | 70.58 | 0.705803536 |
| | 0.00108 | 0.0100 | 0.0006 | 77.45 | 0.774546399 |
| 328 | Blank | 0.061 | 0.003117992 | - | - |
| | 0.000216 | 0.0330 | 0.0020 | 36.76 | 0.36756472 |
| | 0.000432 | 0.0280 | 0.0016 | 49.56 | 0.495560109 |
| | 0.000648 | 0.0230 | 0.0014 | 56.34 | 0.563351388 |
| | 0.000864 | 0.0200 | 0.0011 | 66.22 | 0.662168773 |
| | 0.00108 | 0.0160 | 0.0008 | 73.13 | 0.731309548 |
| 338 | Blank | 0.15 | 0.009129671 | - | - |
| | 0.000216 | 0.1270 | 0.0068 | 25.47 | 0.254738934 |
| | 0.000432 | 0.1040 | 0.0059 | 35.32 | 0.353224146 |
| | 0.000648 | 0.0970 | 0.0057 | 38.08 | 0.380821326 |
| | 0.000864 | 0.0740 | 0.0042 | 53.48 | 0.534787133 |
| | 0.00108 | 0.0610 | 0.0032 | 64.62 | 0.646180033 |
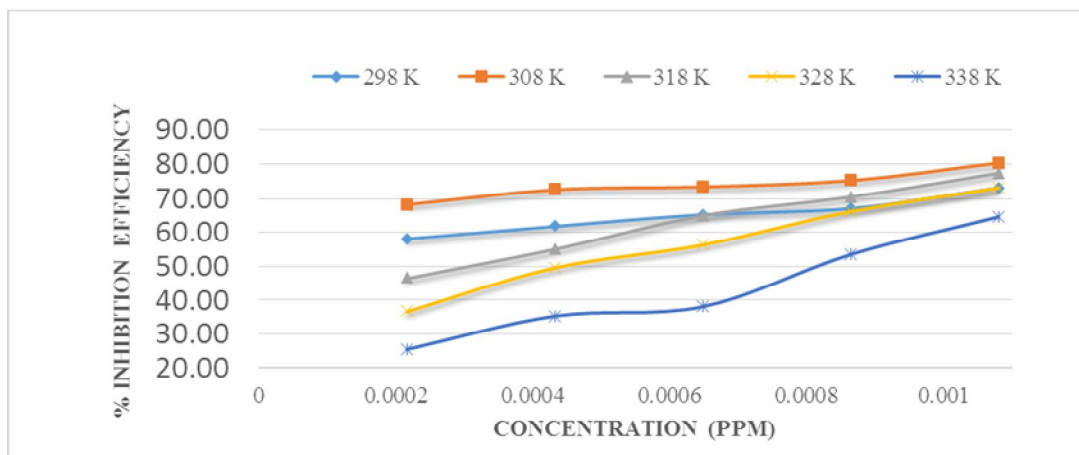
**Fig. 4.** Variation of inhibition efficiency with concentration for AD3 adsorption.
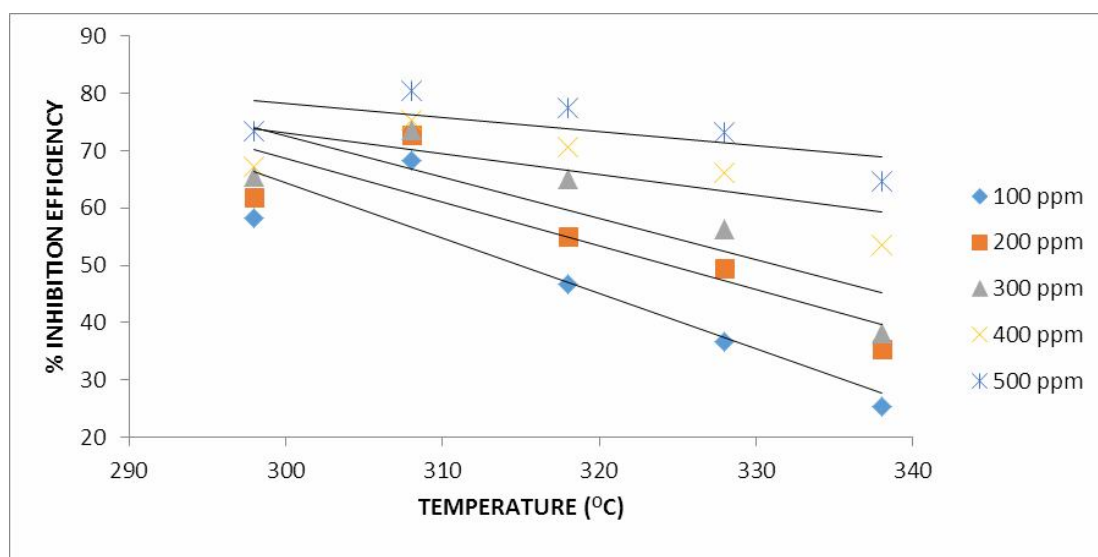


**Fig. 5.** Variation of inhibition efficiency with temperature for AD3 adsorption.

the mild steel as its concentration increases. As shown in Table 1, it could be observed that the corrosion rate decreases considerably from 298 k to 308 k and thereafter increases. An optimum adsorption took place at 308 k and beyond this, desorption takes place. By extension the percentage inhibition efficiency also increased from 298-308 K, beyond this there is decreased inhibition efficiency. Similar observations have been reported in literature for the adsorption of some organic compounds on the surface of

metal [5,16] (Figs. 4 and 5).

**Adsorption Considerations and Thermodynamic Parameters**

The plot of logC *vs*. logθ (298-338 K) generated the data in Table 2 and their plots (Fig. 6). Both linear correlation coefficients ($R^2$) and intercept values are closer to 1, suggesting that the adsorption obeys Freundlich adsorption isotherm [27].
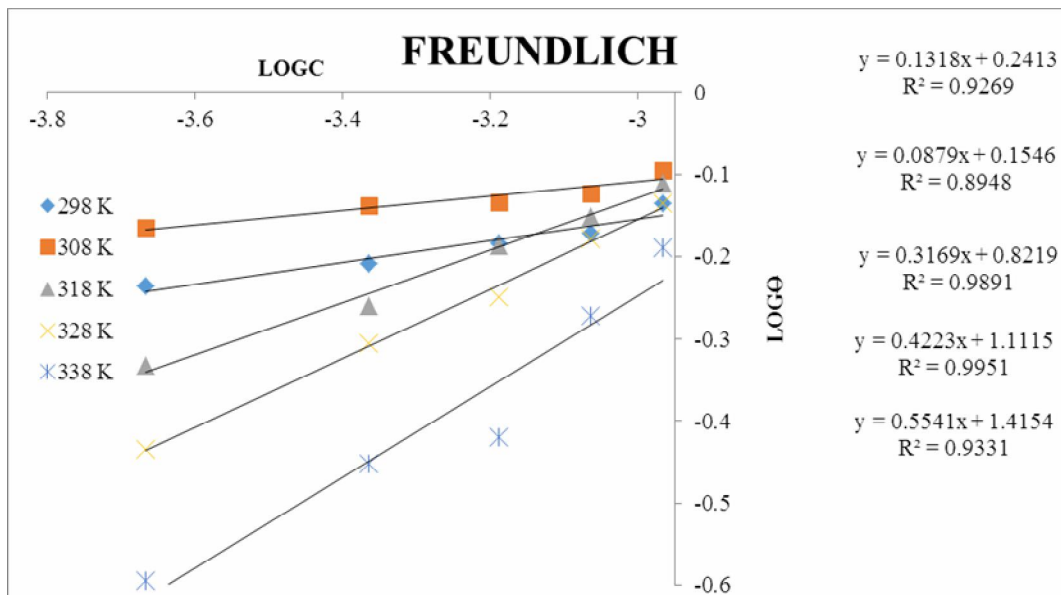
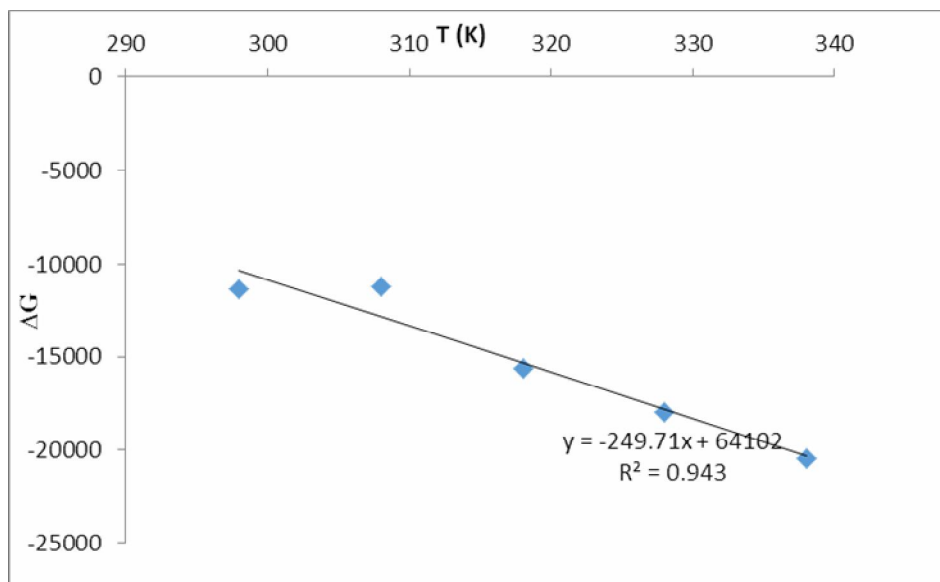**Fig. 6.** Frendulich adsorption isotherm plots for AD3 adsorption.



**Fig. 7.** Determination of enthalpy, $\Delta H$ and entropy, $\Delta S$, of adsorption of AD3.

There is a decrease in the $K_{ads}$ values with temperature, indicating that at relatively lower temperatures, the AD3 molecules were strongly adsorbed on the surface of the mild steel. As the temperature increases, the molecules were desorbed from the surface of the mild steel. From the plot (Fig. 8), $\Delta H^o$ was 64102 kJ mol$^{-1}$ while $\Delta S^o$ was -249.71 kJ mol$^{-1}$ K$^{-1}$.

The results of the thermodynamics study were given by Table 2. The negative value of $\Delta S^o_{ads}$ (-0.250 kJ K$^{-1}$ mol$^{-1}$) obtained for AD3 in this work suggests a reduction in the

**Table 2.** The Data Obtained from Langmuir Adsorption Isotherm and Thermodynamics Study

| Temp. | $R^2$ | Intercept | K | $\Delta G$ (KJ mol$^{-1}$) | Enthalpy (kJ mol$^{-1}$) | Entropy (kJ mol$^{-1}$ K$^{-1}$) |
|---|---|---|---|---|---|---|
| 298 | 0.9269 | 0.2413 | 1.743010 | -11327.4513 | 64.102 | -0.250 |
| 308 | 0.8948 | 0.1546 | 1.427579 | -11196.3616 | - | - |
| 318 | 0.9891 | 0.8219 | 6.635903 | -15622.1981 | - | - |
| 328 | 0.9951 | 1.1115 | 12.927067 | -17931.8986 | - | - |
| 338 | 0.9331 | 1.4154 | 26.025555 | -20445.0085 | - | - |

**Table 3.** Activation Energy, $E_a$ and Pre-exponential Factor A for the Corrosion Process in 0.5 M HCl

| Concentration (M) | Slope | $E_a$ | lnA | A |
|---|---|---|---|---|
| BLANK | -3257 | 27078.7 | 4.5114 | 91.05 |
| 0.000216 | -5095.9 | 42367.31 | 9.6239 | 15121.91 |
| 0.000432 | -4917 | 40879.94 | 8.9031 | 7354.74 |
| 0.000648 | -4893.8 | 40687.05 | 8.7172 | 6107.06 |
| 0.000864 | -4240.8 | 35258.01 | 6.4919 | 659.78 |
| 0.00108 | -4100.7 | 34093.22 | 5.8097 | 333.52 |

translational degrees of freedom, that is, an increased order as the AD3 molecules in the bulk solution are been adsorbed on the metal surface [18]. Generally, for an endothermic adsorption process, $\Delta H^o_{ads}$ is always greater than zero ($\Delta H^o_{ads} > 0$) which implies chemisorptions [18]. In this work, the value of $\Delta H^o_{ads}$ for AD3 was 64 kJ mol$^{-1}$, an indication that the adsorption of AD3 on the mild steel follows Chemisorption, and the negative value of $\Delta G^o_{ads}$ obtained suggested spontaneity of adsorption process.

Activation energy ($E_a$), enthalpy ($\Delta H$) and entropy ($\Delta S$) of activation were estimated from the plots of $\ln C_R$ *vs.* 1/T and $\ln(C_R/T)$ *vs.* 1/T (Figs. 9 and 10), respectively. These values are given in Tables 3 and 4. The estimated values of $\Delta H$ were positive both in the absence and presence of the

inhibitors indicating endothermic nature of the mild steel dissolution [19,20]. The negative values of $\Delta S$ implies activated complex was formed and it represents an associative process. This indicates that there is a decrease in entropy in the reaction from the reactants to the activated complex [21].

**Tafel Polarization Measurements**

The corrosion potential ($E_{corr}$), corrosion current density ($I_{corr}$), anodic Tafel slope ($\beta_a$), cathodic Tafel slope ($\beta_c$) and %IE were obtained (Table 5), Fig. 10. The inhibition efficiency is calculated from the value of corrosion current density evaluated from extrapolation method, using Eq. (10) [22].
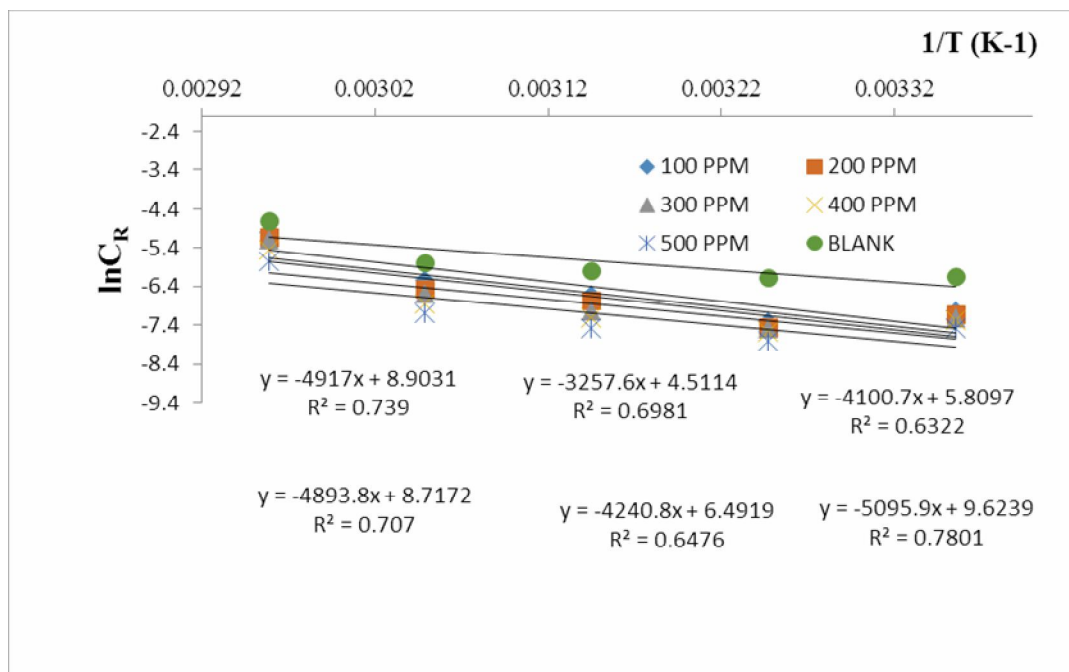
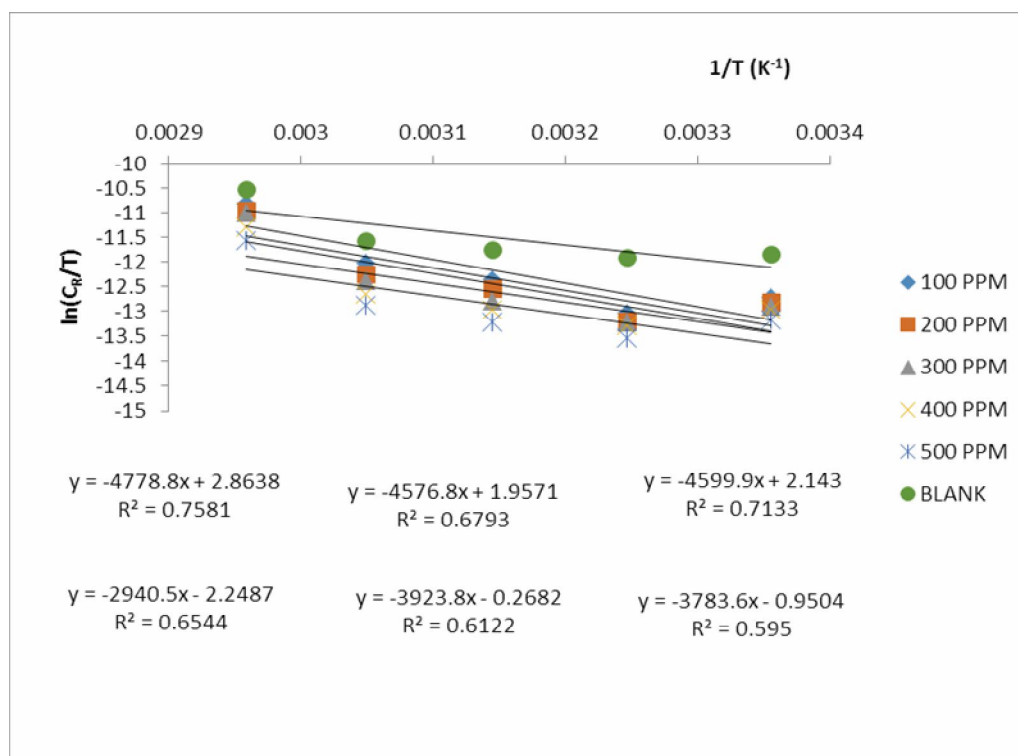**Fig. 8.** Apparent activation energy determination for the corrosion process.



**Fig. 9.** Transition state determination of enthalpy and entropy of activation in 0.5 M HCl in the absence and presence of AD3.

**Table 4.** Transition State Parameters

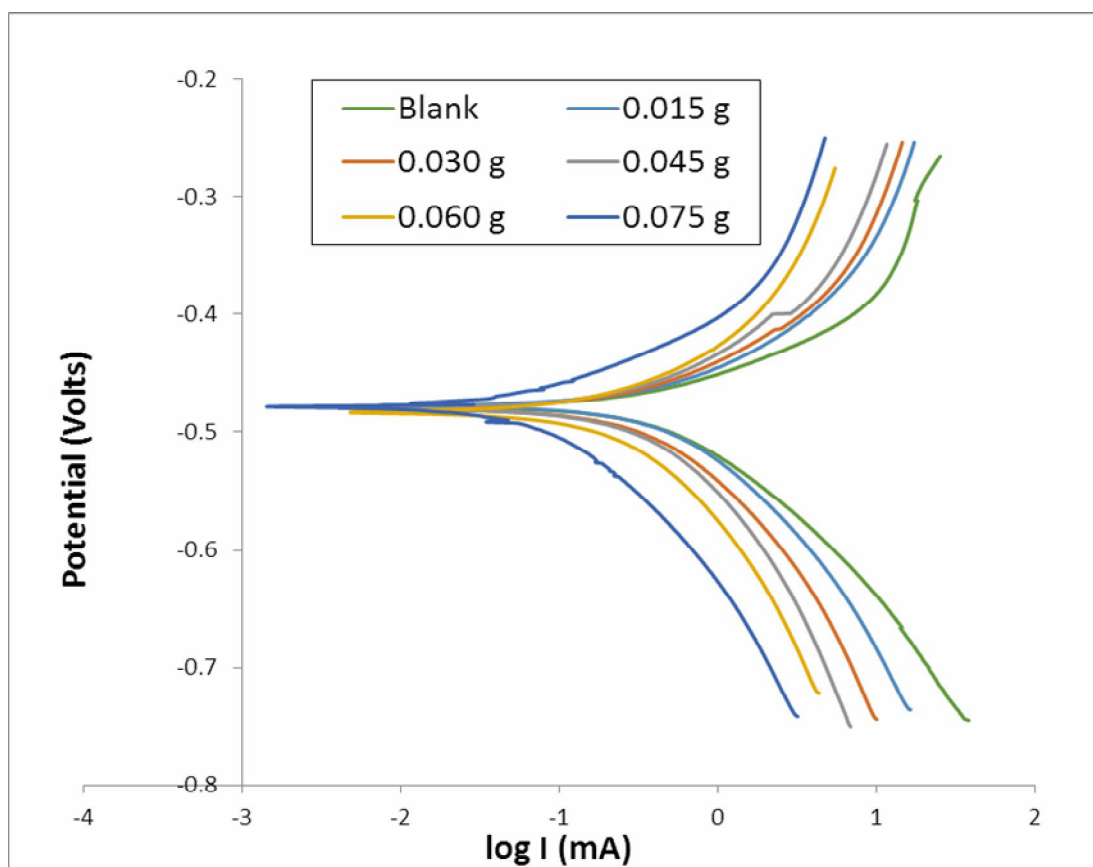| Concentration (M) | Slope | Intercept | Enthalpy ($J\ mol^{-1}$) | Entropy ($J\ mol^{-1}$) |
|---|---|---|---|---|
| BLANK | -2940.5 | -2.2487 | 24447.317 | -216.24 |
| 0.000028 | -4778.8 | 2.8638 | 39730.943 | -173.73 |
| 0.000056 | -4599.9 | 2.143 | 38243.569 | -179.72 |
| 0.000084 | -4576.8 | 1.9571 | 38051.515 | -181.27 |
| 0.000112 | -3923.8 | -0.2682 | 32622.473 | -199.77 |
| 0.00014 | -3783.6 | -0.9504 | 31456.850 | -205.44 |



**Fig. 10.** Polarization curve of the mild steel in 0.5 M HCl in the absence and presence of AD3.

**Table 5.** Polarization Parameters and Inhibition Efficiencies of AD3 on Mild Steel

| Amount (g) | $E_{CORR}$ (mV) | Bc (mV) | Ba (mV) | $C_R$ (mmpy) | Icorr (μA) | IE (%) |
|---|---|---|---|---|---|---|
| blank | -478.62 | 143.5 | 107.7 | 7.51724 | 740.062 | - |
| 0.015 | -478.76 | 162.3 | 123.3 | 6.50633 | 640.539 | 13.45 |
| 0.030 | -481.76 | 185.9 | 126.9 | 5.73991 | 565.086 | 23.64 |
| 0.045 | -480.42 | 214.7 | 133.6 | 5.32353 | 524.094 | 29.18 |
| 0.060 | -484.41 | 205.6 | 149.2 | 3.73773 | 367.974 | 50.28 |
| 0.075 | -479.14 | 155.3 | 101.9 | 1.08693 | 107.007 | 85.54 |

Results from the Tafel curve (Fig. 10) revealed that AD3 is a mixed-type inhibitor (both cathodic and anodic) [23]. The corrosion rate decreases with respect to increase in the inhibitor loading resulting in relative increase in the inhibition efficiency (Table 5). This observation is due to the increase in the coverage of the surface of the mild steel as the concentration of the inhibitor increases from 0.015 g to 0.075 g.

**SEM-EDX Analysis**

Figure 11 showed the SEM image of the mild steel surface. The polished mild steel before immersion (Fig. 11a) looks smoother with some little scratches on the surface. However, the mild steel after immersion in 0.5 M HCl for 6 h showed an aggressive attack of the corroding medium (Fig. 11b). Figure 11c also showed that there is much less damage on the mild steel surface in the presence of the inhibitor confirming the inhibiting capability.

Energy dispersed X-ray (EDX) analysis gives the percentage of the element present on the surface of the mild steel. From the EDAX analysis, the presence of oxygen and iron suggested the presence of iron oxide or hydroxide. Figure 12, showing the presence of the peaks of nitrogen, chlorine, silicon, carbon, and sulphur, suggested the adsorption of the inhibitor on the mild steel.

**Quantum Chemical Analysis**

$\Delta E$ value for AD3 is 3.63 eV, implying that there is obviously an electron donation from AD3 to the metal surface as evidenced by the high $E_{HOMO}$ (-6.93 eV). A low $E_{LUMO}$ of -2.95 eV implies the ability of the inhibitor to accept electrons from the $d$ orbitals of the metal. AD3 has the $\Delta N$ value of 0.6, confirming that AD3 is effective. A molecule is termed a good inhibitor if $\Delta N < 3.6$ [4,5], this is a direct consequence of its low hardness value (1.84 eV) and high softness value (0.54 eV$^{-1}$). The $\omega$ value (6.58) also confirms that there is an appreciable reactivity in AD3 molecule. All these are provided in Table 6. The results from the theoretical investigation agreed well with experimental observations [24].

**CONCLUSIONS**

AD3 was synthesized and characterized. Its ability to inhibit corrosion of mild steel was investigated using gravimetric and electrochemical methods. The results obtained presented AD3 as an efficient potential inhibitor for mild steel dissolution in aggressive media. Its inhibition efficiency increases with increase in concentration and decreases as the temperature increases. Electrochemical measurements revealed that AD3 is a mixed-type organic inhibitor. This is confirmed by the results of potentiodynamic polarization. The adsorption mode obeyed Freundlich adsorption isotherm. It is an endothermic and entropy-reducing process, while the adsorption mechanism follows chemisorption. The theoretical results were consistent with the available experimental data. AD3, therefore, could be used as a corrosion resistant agent in the oil and gas industry.
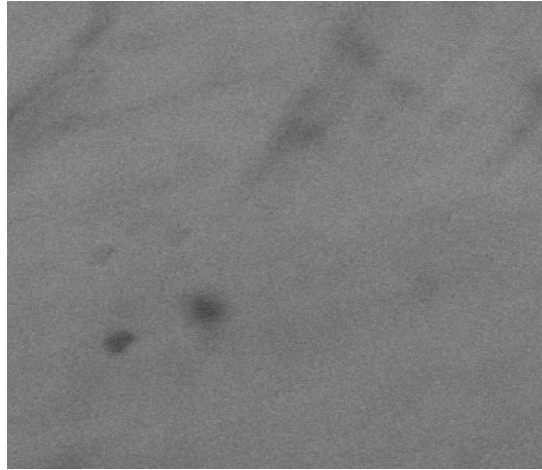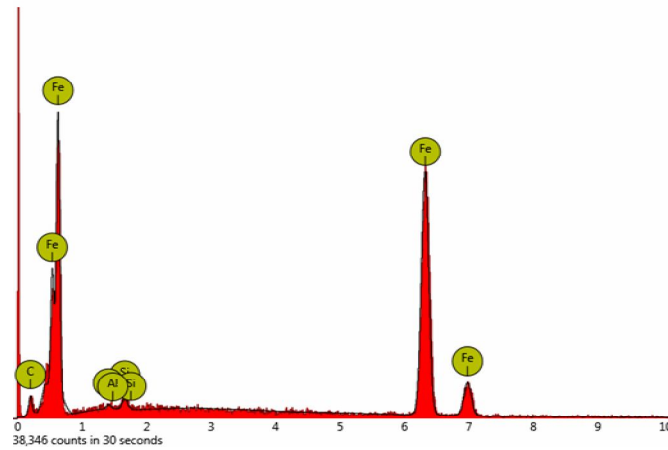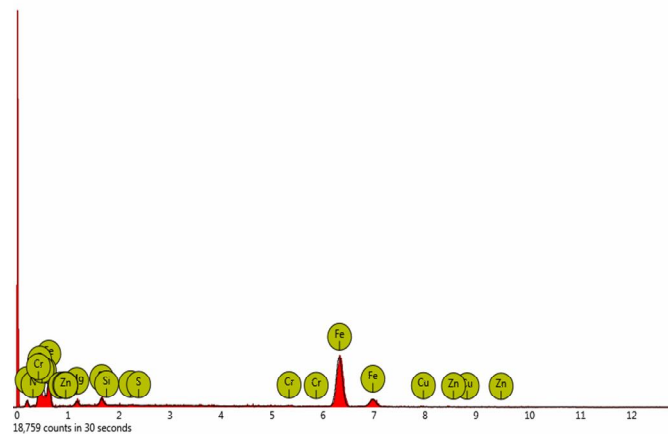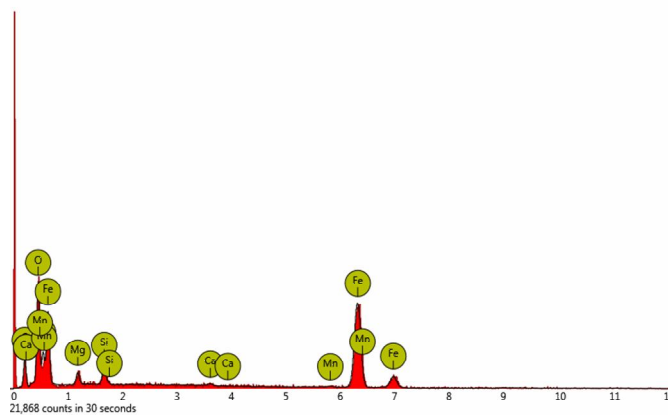
**(a)**
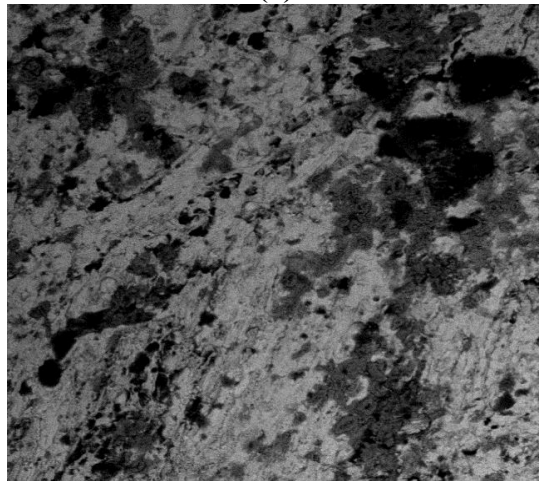


**(b)**
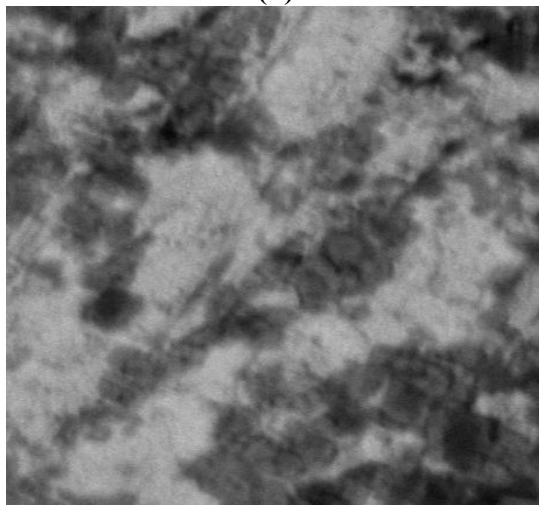


**(c)**

**Fig. 11.** (a) SEM image of the polished mild steel, (b) SEM image of the mild steel exposed to 0.5 M HCl, and  (c) SEM image of mild steel in the presence of 200 PPM extract.

**(a)**



**(b)**



**(c)**

**Fig. 12.** (a) EDX image of polished mild steel, (b) EDX image of mild steel exposed to 0.5 M HCl, and (c) EDX image of mild steel in the presence of 200 PPM extract.

**Table 6.** Quantum Chemical Parameters of AD3 Dye

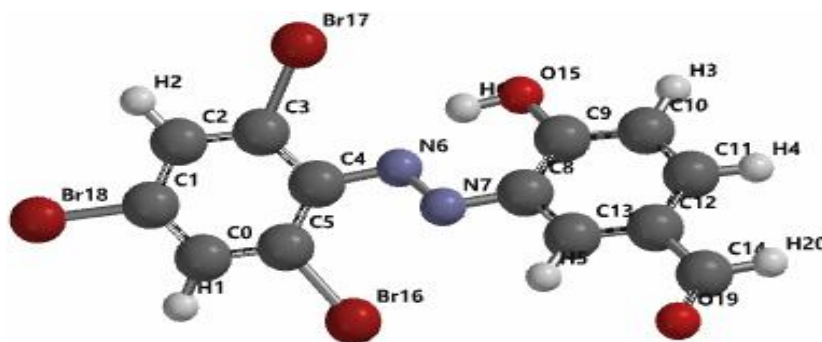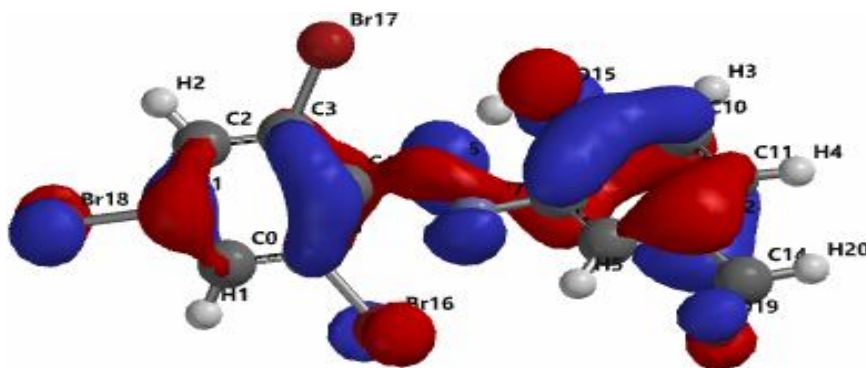| Parameters | $E_{HOMO}$ (eV) | $E_{LUMO}$ (eV) | $\Delta E$ (eV) | $\eta$ (eV) | $\delta$ (eV$^{-1}$) | $\chi$ | $\omega$ | $\mu$ (D) | $\Delta N$ | A (eV) | I (eV) |
|---|---|---|---|---|---|---|---|---|---|---|---|
| AD3 | -6.63 | -2.95 | 3.63 | 1.84 | 0.54 | 4.79 | 6.58 | 2.50 | 0.60 | 6.63 | 2.95 |



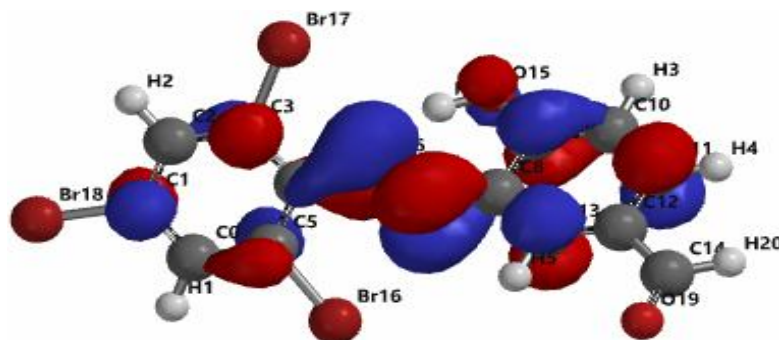**Fig. 13a.** Optimized structure of AD3.



**Fig. 13b.** HOMO map of AD3.



**Fig. 13c.** LUMO map Of AD3.

## REFERENCES

[1]     Bilgic, S.; Sahin M. The corrosion inhibition of austenitic chromium-nickel steel in $H_2SO_4$ by 2-butyn-1-ol. *Mat. Chem. Phys.* **2015**, *70*, 290-295. DOI: 10.1016/S0254-0584(00)00534-4.

[2]     Chandrabhan, V.; Quraishi, M. A.; Ebenso, E. E., Microwave and ultrasound irradiations for the synthesis of environmentally sustainable corrosion inhibitors: An overview. *Sustain. Chem. Pharm.* **2018**, *10*, 134-147. DOI:10.1016/j.scp.2018.11.001.

[3]     Obot, I.; Edouk, U. M., Benzimidazole: small planar molecule with diverse anticorrosion potentials. *J. Mol. Liq.* **2017**, *246*, 66-90. DOI: 10.1016/j.molliq.2017.09.041.

[4]     Oyeneyin, O. E., Structural and solvent dependence of the electronic properties and corrosion inhibitive potentials of 1,3,4-thidiazole and its substituted derivatives-A theoretical investigation. *Phys. Sci. Int. J.* **2017**, *16*, 1-8. DOI: 10.9734/PSIJ/2017/36555.

[5]     Amoko, S. J.; Akinyele, O. F.; Oyeneyin, O. E.; Olayanju, D. S.; Aboluwoye, C. O., Synthesis, characterization and computational studies on the corrosion inhibitive potentials of (e)-3-(2-p-tolyldiazenyl)-1-nitrosonaphthalen-2-ol. *Leon. J. Sci.* **2018**, *33*, 29-48.

[6]     Fouda, A. S.; Elmorsi, M. A.; Elmekkawy, A., Eco-friendly chalcones derivatives as corrosion inhibitors for carbon steel in hydrochloric acid solution. *Afric. J. Pure Appl. Chem.* **2013**, *7*, 337-349. DOI: 10.5897/AJPAC2013.0520.

[7]     Kumari, P. P.; Shetty, P.; Rao, S. A., Electrochemical measurements for the corrosion inhibition of mild steel in 1 M hydrochloric acid by using an aromatic hydrazide derivative. *Arab. J. Chem.* **2017**, *10*, 653-663. DOI: 10.1016/j.arabjc.2014.09.005.

[8]     Al-Fakih, A. M.; Abdallah, H. H.; Maarof, H.; Aziz, M., Experimental and quantum chemical calculations on corrosion inhibition of mild steel By two furan derivatives. *J. Teknol.* **2016**, *78*, 121-125. DOI: 10.11113/jt.v78.9242.

[9]     Oyeneyin, O. E.; Adejoro, I. A.; Ogunyemi, B. T.; Esan, O. T., Structural and solvent dependence on the molecular and nonlinear optical properties of 10-octyl thiophene-based phenothiazine and substituted derivatives-a theoretical approach. *J. Taibah Univ. Sci.* **2018**, *12*, 483-493. DOI: 10.1080/16583655.2018.1485274.

[10]    Oyeneyin, O. E.; Adejoro, I. A.; Esan, T. O., Substituent effects on the structural and nonlinear Optical Properties of 1-[4-({(E)-[4 (methylsulfanyl)phenyl] methylidene} amino) phenyl] ethanone and some of its substituted derivatives-a theoretical method. *Phys. Chem. Res.* **2018**, *6*, 667-683. DOI: 10.22036/pcr.2018.119109.1471.

[11]    Ahmadi, R. A.; Amani, S., Synthesis, spectroscopy, thermal analysis, magnetic properties and biological activity studies of Cu(II) and Co(II) complexes with schiff base dye ligands molec. **2012**, *17*, 6434-6448. DOI: 10.3390/molecules17066434.

[12]    Chen, W.; Luo, H. Q.; Li, N. B., Inhibition effects of 2,5-dimercapto-1,3,4-thiadiazole on the corrosion of mild steel in sulphuric acid solution. *Corr. Sci.* **2011**, *53*, 3356-3365. DOI: 10.1016/j.corsci.2011.06.013.

[13]    Ituen, E.; Mkpenie V.; Moses E.; Obot I., Electrochemical kinetics, molecular dynamics, adsorption and anticorrosion behavior of melatonin biomolecule on steel surface in acidic medium. *Bioelect.* **2019**, *129*, 42-53. DOI: 10.1016/j.bioelechem.2019.05.005.

[14]    Evans, J. C., The vibrational spectrum of phenol and phenol-OD. *Spectroc. Acta.* **1960**. *16*, 1362-1392. DOI: 10.1016/S0371-1951(60)80011-2.

[15]    Sun, Z.; Zhao, J.; Ju, X.; Xia, Q., Effect of nitrogen cation as electron trap at the π-linker on properties of p-type photosensitizers: DFT study. *Molec.* **2019**. *24*, 3134. DOI: 10.33390/molecules24173134.

[16]    Obot, I. B.; Obi-Egbedi N. O.; Umoren S. A., Antifungal drugs as corrosion inhibitors for aluminium in 0.1 M HCl. *Corr. Sci.* **2009**, *51*, 1868-1875. DOI:10.1016/j.corsci.2009.05.017.

[17]    Deng, S.; Li, X., Inhibition by Jasminum nudiflorum lindl. leaves extract of the corrosion of aluminium in HCl solution. *Corros. Sci.* **2012**, *64*, 253-262. DOI: 10.1016/j.corsci.2012.07.017.

[18] Desimone, M. P.; Gordillo, G.; Simison, S. N., The effect of temperature and concentration on the corrosion inhibition mechanism of an amphiphilic amido-amine in $CO_2$ saturated solution. *Corr. Sci.* **2011**, *53*, 4033-4043. DOI: 10.1016/ j.corsci.2011.08.009.

[19] Obot, I. B.; Obi-Egbedi N. O. Fluconazole as an inhibitor for aluminium corrosion in 0.1 M HCl. *Colloids Surf. A: Physic. Engineer. Asp.* **2008**, 330, 207-212. DOI: 10.1016/j.colsurfa.2008.07.058.

[20] Dehri, I.; Ozcan, M., The effect of temperature on the corrosion of mild steel in acidic media in the presence of some sulphur-containing organic compounds. *Mater. Chem. Phys.* **2006**, *98*, 316-323. DOI: 10.1016/j.matchemphys.2005.09.020.

[21] Saliyan, R.; Adhikari, A. V., Inhibition of corrosion of mild steel in acid media by N'-benzylidene-3-(quinolin-4-ylthio) propanohydrazide. *Bullet. Mat. Sci.* **2008**, *31*, 699-711. DOI: 10.1007/s12034-008-

0111-4.

[22] He, X.; Jiang, Y.; Li, C.; Wang, W.; Hou, B.; Wu, L., Inhibition properties and adsorption behavior of imidazole and 2-phenyl-2-imidazoline on AA5052 in 1.0 M HCl solution. *Corr. Sci.* **2014**, *83*, 124-136. DOI: 10.1016/j.corsci.2014.02.004.

[23] Hu, J.; Zeng, D.; Zhang, Z.; Shi T.; Song G. L,; Guo X. 2-Hydroxy-4-methoxy-acetophenone as an environment-friendly corrosion inhibitor for AZ91D magnesium alloy. *Corr. Sci.* **2013**, *74*, 35-43. DOI: 10.1016/j.corsci.2013.04.005.

[24] Ogunleye, O. O.; Arinkoola, A. O.; Eletta, O. A.; Agbede, O. O.; Osho, Y. A.; Morakinyo, A. F., Green corrosion inhibition and adsorption characteristics of Luffa cylindrica leaf extract on mild steel in hydrochloric acid environment. *Helyion.* **2020**, *6,* 1-12. DOI: 10.1016/ j.heliyon.2020.e03205.